

Tuning the Structural and the Magnetic Properties of BiFeO₃ Magnetic Nanoparticles

Antonios Makridis,* Eirini Myrovali, Despina Sakellari, and Mavroeidis Angelakeris

The explosive expansion of multiferroics literature in recent years demonstrates the fast-growing interest in this field. Although bismuth ferrite is one of the most extensively investigated multiferroic compounds combining magnetoelectric, i.e., antiferromagnetic and ferroelectric features at room temperature, the challenge of producing single-phase particles remains because the role of multiple synthetic parameters must be unraveled. Herein, the facile synthetic route of aqueous coprecipitation is selected as the first synthetic step, followed by a 700 °C annealing stage to synthesize bismuth ferrite nanoparticles (NPs). This article aims to clarify the influence of ingredients such as precursors: base solution, acid and the Bi/Fe molar ratio, and the role of synthetic parameters such as pH level and reaction temperature toward higher yields of purer crystalline phases. Both structural and magnetic features' performance outline the significance of both stages on forming BiFeO₃ single-phase NPs with the absence of any secondary bismuth oxide phases, a crucial issue for multiferroic features at room temperature.

1. Introduction

Materials that simultaneously possess two or more ferroic-order parameters have become a hot topic of research in recent years.^[1,2] Such a combinatory behavior between magnetic and electric properties opens the pathway of novel devices provided magnetic and electric orders can be mutually controlled. Among the different types of multiferroic compounds, bismuth ferrite (BiFeO₃) stands out due to its unique room-temperature features: antiferromagnetism and ferroelectricity.^[1–6] Therefore, extensive research has been devoted to bismuth iron oxide (BFO)-based materials in a variety of forms, including bulk ceramics, thin films, and nanosized compounds^[7–9] with direct applicability either as magnetoelectric and photovoltaic materials^[5–13] or more

recently as multifunctional biomedical probes, i.e., sensitizers for radiotherapy and heat mediators for hyperthermia.^[14] Despite the multiple reviews on the synthesis of BiFeO₃, an equilibrium compound,^[15,16] by different methodologies and corresponding “optimal” conditions for a single-phase compound free from impurity phases, this remains a hard-to-achieve task.^[17] The metastability during synthesis is proposed as a reason for the inability to acquire this compound uncontaminated from secondary Bi₂O₃–Fe₂O₃ biproducts.^[18] Additional constraints for the success of a solid phase synthesis process may be attributed to nonstoichiometry and variations in the homogeneity region with increased temperature.^[19] Meanwhile, the activation of BiFeO₃ formation seems to depend on the chemical stoichiometry of the initial mixture.^[20] Thus, several sequential transformations occur when BiFeO₃ is synthesized from Bi₂O₃ and Fe₂O₃ by the solid-state chemical reaction method.

Intermediate phases like Bi₂Fe₄O₉ and Bi₂₅FeO₃₉, not possessing magnetoelectric features, are considered as secondary products, hindering the high yield of single-phase BiFeO₃ nanoparticles (NPs).^[21,22] It is well known that formation kinetics of NP synthesis can be controlled by tuning the temperature during the annealing stage of synthesis or by changing the precursor's ratio.


In this work, aqueous coprecipitation method is proposed as a first synthetic stage, sequenced by 2 h annealing, under argon (Ar) atmosphere at 700 °C, approximating the optimal calcination temperature to form single-phase BiFeO₃ NPs with a direct impact on magnetic features. Aiming to fill the existing literature gap, the effect of Bi/Fe ratio to the stoichiometry of the final BFO product and its consequence on collective magnetic features is the first step of our work. Furthermore, we examine how alternative precursors (namely nitric acid instead of hydrochloric acid) or temperature/pH tuning may control the content of impurity nonstoichiometric bismuth oxide phases and, finally, if the NPs' magnetic properties could be tuned by adjusting the main reaction parameters.

2. Experimental Section

Preparing samples using different Bi/Fe molar ratio (samples BFO1–BFO3) to evaluate its impact on the structure and the magnetic properties of bismuth ferrite NPs was the first synthesis attempt of this work. Next, reaction temperature and

Dr. A. Makridis, Dr. E. Myrovali, Dr. D. Sakellari, Prof. M. Angelakeris
School of Physics
Faculty of Sciences
Aristotle University of Thessaloniki
54124 Thessaloniki, Greece
E-mail: anmakrid@physics.auth.gr

Dr. A. Makridis, Dr. E. Myrovali, Dr. D. Sakellari, Prof. M. Angelakeris
Magnetic Nanostructure Characterization: Technology and Applications
(MagnaCharta)
Center for Interdisciplinary Research and Innovation (CIRI-AUTH)
57001 Thessaloniki, Greece

 The ORCID identification number(s) for the author(s) of this article can be found under <https://doi.org/10.1002/pssb.202000005>.

DOI: 10.1002/pssb.202000005

pH level were tuned (sample BFO4), as an attempt to investigate their impact to the final bismuth ferrite product. As it had been mentioned before, the role of the precursors used during synthesis (the base solution as well as of the acid type) and how they affect the final product was the last synthesis goal of this study.

2.1. Synthesis

NPs samples were prepared by aqueous coprecipitation method and all chemicals reagents used in the following synthesis experiments were of high purity without any further purification. All chemicals were purchased from Riedel-De Haen, VWR Chemicals, AnalR Normapur, and PanReac-AppliChan chemical companies. Six BFO samples were prepared for the purposes of this work, named BFO1–BFO6. Samples' notation together with their structural and magnetic features appears in **Table 1**.

To investigate the role of Bi/Fe molar ratio in the final product of bismuth ferrite NPs, three samples (BFO1, BFO2, and BFO3) with different Bi/Fe molar ratio were synthesized. For sample BFO1, 0.83 g of bismuth nitrate pentahydrate ($\text{Bi}(\text{NO}_3)_3 \cdot 5\text{H}_2\text{O}$) and 2 g of iron nitrate nonahydrate ($\text{Fe}(\text{NO}_3)_3 \cdot 9\text{H}_2\text{O}$) were dissolved in 150 mL of distilled water, keeping the Bi/Fe molar ratio at 1/3. For BFO2 sample, 7.47 g of bismuth nitrate pentahydrate ($\text{Bi}(\text{NO}_3)_3 \cdot 5\text{H}_2\text{O}$) and 2 g of iron nitrate nonahydrate ($\text{Fe}(\text{NO}_3)_3 \cdot 9\text{H}_2\text{O}$) were dissolved in 150 mL of distilled water, keeping the Bi/Fe molar ratio at 3/1. The target for the third sample (BFO3) was to prepare BFO NPs with molar ratio 1/1. For this reason, 2.5 g of bismuth nitrate pentahydrate ($\text{Bi}(\text{NO}_3)_3 \cdot 5\text{H}_2\text{O}$) and 2 g of iron nitrate nonahydrate ($\text{Fe}(\text{NO}_3)_3 \cdot 9\text{H}_2\text{O}$) were dissolved in 150 mL of distilled water. In all samples, the mixture was stirred at room temperature for about 2 h. Then, 20 mL of HCL (37%) was added drop wise and stirring was continued until the solution changed into transparent liquid. In general, in aqueous coprecipitation, the pH of the coprecipitation mixture has a crucial effect on the chemical, structural, and magnetic properties of the final material. The pH of the solution was controlled by immediately adding drops of 1 M NaOH solution, until the desired value 12 was reached. Reaction temperature was kept constant at 84 °C in all three synthesis attempts. The precipitated orange-colored product was kept at room temperature for about 24 h and was washed 5 times with distilled water to remove nonreacting excesses. The final powder product was annealed at Ar atmosphere at 700 °C for 2 h.

Table 1. Structural and magnetic properties of BFO samples.

Samples	(Synthesis) molar ratio (Bi/Fe)	(SEM) atomic ratio (Bi/Fe)	(XRD) size [nm]	M_s ($\text{A m}^2 \text{kg}^{-1}$)	H_c [mT]
BFO1	1/3	0.61 ± 0.04	29.0 ± 9.5	5.30	14.0
BFO2	3/1	5.42 ± 0.38	21.0 ± 4.5	0.00	0.5
BFO3	1/1	1.67 ± 0.12	19.0 ± 3.2	0.40	5.0
BFO4	1/1	1.79 ± 0.13	42.0 ± 6.3	0.20	20.0
BFO5	1/1	1.40 ± 0.10	38.0 ± 12.3	0.20	32.0
BFO6	1/1	1.59 ± 0.14	34.0 ± 9.9	0.05	0.2

As it is mentioned before, temperature and pH level are two key factors in chemical reactions. To study the effect of the reaction temperature and pH level in the synthesis of bismuth ferrite NPs, a fourth synthesis was also attempted (BFO4 sample), where the Bi/Fe molar ratio was kept at 1/1 and this was the last sample that hydrochloric acid ($\text{H}_2\text{O}:\text{HCl}$) was used as synthesis acid. For the preparation of this sample, 7.76 g of bismuth nitrate pentahydrate ($\text{Bi}(\text{NO}_3)_3 \cdot 5\text{H}_2\text{O}$) and 6.46 g of iron nitrate nonahydrate ($\text{Fe}(\text{NO}_3)_3 \cdot 9\text{H}_2\text{O}$) were dissolved in 150 mL of distilled water. Apart from the reaction temperature and the pH level that reached 70 °C and the value of 10, respectively, all the previous synthesis conditions were kept the same.

To investigate the effect of acids as well as base solution used during synthesis on the structure and magnetism of BFO NPs, a fifth BFO sample (BFO5 sample) was synthesized. Nitric acid (HNO_3) was used during preparation of the sample, instead of hydrochloric acid ($\text{H}_2\text{O}:\text{HCl}$). Meanwhile, denser base solution of NaOH (2 M) was added in this synthesis procedure instead of the 1 M NaOH base solution. Concerning the synthesis procedure, 2 g of bismuth nitrate pentahydrate ($\text{Bi}(\text{NO}_3)_3 \cdot 5\text{H}_2\text{O}$) were dissolved in 100 mL of distilled water. Solution was kept under stirring and at a constant temperature of 70 °C. Afterward, nitric acid (HNO_3 ; 65%) was added into the solution, until it became transparent. Separately, 1.66 g of iron nitrate nonahydrate ($\text{Fe}(\text{NO}_3)_3 \cdot 9\text{H}_2\text{O}$) were added into 50 mL of distilled water. The two solutions were then mixed, whereas temperature was constant at 70 °C, under mild stirring. At that time, NaOH (2 M) solution was added drop by drop, until pH reached the value 12. Drying and stirring procedures were conducted under the same conditions as in the previous four samples.

Because annealing step close to 700 °C was proposed^[23] as a mandatory step to attenuate the impurity phase content in the final product of bismuth ferrite NPs, the as-prepared BFO6 sample provided the reference sample for the annealing process.

2.2. Methods

X-ray diffraction patterns were obtained using a Philips PW 1710 diffractometer with Cu K α as a radiation source ($\lambda = 1.54242 \text{ \AA}$) in the 2θ range from 20° to 90° with scanning step width of 0.05° and 3 s scanning time per step. The structural observation and micromorphology were conducted with a JEOL JSM 840A scanning electron microscopy (SEM) equipped with an OXFORD INCA energy-dispersive X-ray analyzer (EDS) for elemental analysis to measure Bi/Fe atomic ratio. The magnetization hysteresis curves (M versus H) at room temperature were obtained by vibrating sample magnetometry (VSM; 1.2H/CF/HT Oxford Instruments VSM).

3. Results and Discussion

In a typical synthetic attempt of BFO NPs, at the initial stage, $\text{Bi}_{25}\text{FeO}_{39}$ is formed with maximizing content at $\approx 500^\circ\text{C}$. Then, BiFeO_3 phase intensifies sharply at $\approx 600^\circ\text{C}$, whereas further increase in the reaction temperature leads to the formation of secondary phases such as $\text{Bi}_2\text{Fe}_4\text{O}_9$ along with BiFeO_3 and $\text{Bi}_{25}\text{FeO}_{39}$ phases. The occurrence of $\text{Bi}_2\text{Fe}_4\text{O}_9$ and $\text{Bi}_{25}\text{FeO}_{39}$ formation during BiFeO_3 synthesis depends on the

quality of the initial reagents.^[24] Consequently, the difficulty to synthesize single-phase BiFeO₃ arises from the fact that Bi₂Fe₄O₉ and Bi₂₅FeO₃₉ are thermodynamically more stable than BiFeO₃.^[21,22] Herein, we examine different synthetic aspects in conjunction with the final NPs phase. More specifically, the role of Bi/Fe molar ratio, of the synthesis parameters, such as pH level and reaction temperature, as well as of the precursors (the base solution and the type of acid) used during synthesis were evaluated regarding their influence to the final product (their impact to the structure and magnetic properties of the final bismuth ferrite NPs). The way how each parameter affects the structure as well as the magnetic properties of the final NPs is thoroughly analyzed in the subsequent subsection.

3.1. The Role of Bi/Fe Molar Ratio

The first target of this work is to determine the adequate, from structural point of view, Bi/Fe molar ratio, because multiferroic NPs possess optimum magnetoelectric properties when stoichiometric bismuth iron oxide phase (BiFeO₃) dominates in their structure.^[19,23] To examine how different stoichiometry may affect the structural and magnetic properties of BiFeO₃ NPs, three different synthetic attempts were followed, aiming to three different Bi/Fe molar ratio—1/3 in sample BFO1, 3/1 in sample BFO2, and 1/1 in sample BFO3—as shown in Table 1.

Figure 1 shows the corresponding X-ray powder diffraction (XRD) patterns for postsynthetic annealed samples where in Figure 1a, from bottom to top, we have red: BFO1, green: BFO2, and blue: BFO3 patterns corresponding to 1/1, 1/3, and 3/1 Bi/Fe ratio, respectively. Vertical color bars demonstrate the main peaks of the existing phases, with their length

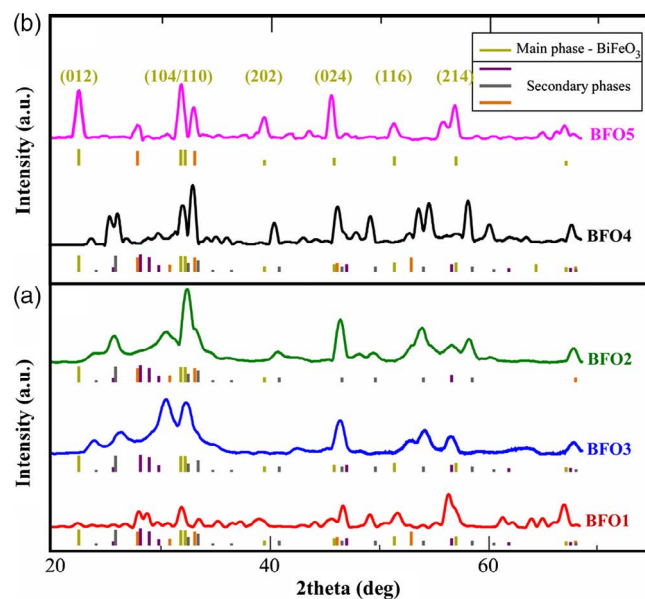


Figure 1. X-ray diffractograms of BFO samples synthesized a) using different nominal Bi/Fe molar ratio under the same synthesis conditions (red: BFO1 [1/3], green: BFO2 [3/1], and blue: BFO3 [1/1]) and b) using the same nominal Bi/Fe ratio 1/1 under different synthesis conditions (black: BFO4 [hydrochloric acid + weak base], pink: BFO5 [nitric acid + strong base]) all annealed at 700 °C for 2 h under Ar atmosphere.

representing their relative intensity (with respect to main peak in each case). In all cases, peaks coincide with the reference ones for BFO (BiFeO₃: PDF #71-2494, olive color vertical lines). Additional peaks attributed to secondary phases are formed during the fabrication process (BiOCl: PDF #06-0249, gray color peaks) appear in all three samples (mainly in BFO2), whereas in BFO1 and BFO3 samples, the nonstoichiometric bismuth iron oxide phases also exist, i.e., Bi₂Fe₄O₉: PDF #25-0090 and Bi₄₆Fe₂O₇₂: PDF #20-0170 for sample BFO1 and Bi₂Fe₄O₉: PDF #25-0090 for sample BFO3. The existence of BiOCl phase is connected with the hydrochloric acid used during the synthesis. In contrast, the presence of bismuth iron oxide phases such as Bi₄₆Fe₂O₇₂ (PDF #20-0170) and Bi₂Fe₄O₉ (PDF #25-0090) may be attributed on the kinetics of formation, due to which, some impurity phases are always obtained along with the stoichiometric BiFeO₃ phase (PDF #71-2494), as the major phase during the synthesis of BFO MNPs. Such impurity phases exist in multiple relevant reports.^[19,25–28]

Meanwhile, the desirable stoichiometric BiFeO₃ phase (main reference peaks are colored as olive color lines—BiFeO₃: PDF #71-2494) exists in all five samples. Regarding the samples synthesized with different Bi/Fe stoichiometry (BFO1, BFO2, and BFO3), BiFeO₃ phase appears with more intense in BFO3 sample (blue curve with 1/1 Bi/Fe nominal ratio). In agreement with the literature results,^[29–31] 1/1 Bi/Fe presented here as the optimum molar ratio. Comparing with the literature, it has been previously shown^[31] that pure-phase BiFeO₃ was observed for Bi/Fe ratios of 1.0–1.1, whereas bismuth-deficient and bismuth-rich phases were observed along with pure BiFeO₃ for different Bi/Fe ratio. Crystallite size and crystallinity of the BFO strongly depend on the Bi/Fe ratio, thus affecting the magnetic properties of the NPs, as it is discussed in the subsequent subsection.

3.2. The Role of the Synthesis Parameters and Precursors

Various synthetic attempts of tunable size and morphology BiFeO₃ NPs are proposed, including low-temperature techniques, such as the hydrothermal and coprecipitation method together with subsequent annealing stage.^[19,27,28,32–34] The choice of the precursors has direct impact on the formation, structure, and size of BiFeO₃.^[35,36] Hardy et al.^[36] reported that BiFeO₃ crystallization begins around 400 °C, an increase in the reaction temperature of up to 500–600 °C may yield single-phase BiFeO₃. In contrast, Mikhailov et al.^[37] concluded, after thermodynamic calculations, that the synthesis temperature to produce single-phase BiFeO₃ should not be above 727 °C, that is, above the temperature of the α → Bi₂O₃ transition, as the high entropy of the disordered β-Bi₂O₃ sharply decreases the Gibbs energy of bismuth ferrite formation. The suggested optimal synthesis temperature is around 720 °C. Despite the numerous attempts to synthesize BiFeO₃ NPs, final product is a multiphase micro- or nanopowder, with no distinct reasoning for the multiple-phase formation during BiFeO₃ synthesis.^[38–42]

Keeping the Bi/Fe molar ratio 1/1 as the optimum synthesis ratio to prepare multiferroic NPs, the role of the reaction temperature together with the impact of the base solution as well as of the acid type used during synthesis on the final NPs phase is studied. More specifically, it is examined if the secondary phases'

(BiOCl and the nonstoichiometric bismuth oxides) content can be controlled at the final product by replacing hydrochloric acid with nitric acid.

As shown in Figure 1b, by reducing the reaction temperature and pH at 70 °C and 10, respectively, the secondary phases of bismuth iron oxides and bismoclite still remain in the final product (sample BFO4 presented by black curve), yet at smaller content due to narrower diffraction peaks compared with BFO1–BFO3 respective peaks of Figure 1a. Bismoclite (BiOCl; PDF #06-0249, gray color peaks) appears pronounced in BFO4 sample together with the nonstoichiometric BFO secondary phases ($\text{Bi}_{46}\text{Fe}_2\text{O}_{72}$; PDF #20-0170 and $\text{Bi}_2\text{Fe}_4\text{O}_9$; PDF #25-0090). In contrast, using nitric acid (used in sample BFO5) instead of hydrochloric acid (used in BFO1, BFO2, BFO3, and BFO4 samples) during synthesis appears to act beneficially to the structure of BFO5 sample, because bismoclite phase (BiOCl; PDF #06-0249, gray color peaks) no longer appears. It is noticeable that only bismuth iron oxide phase of $\text{Bi}_{46}\text{Fe}_2\text{O}_{72}$ (orange lines correspond to PDF #20-0170 main peaks) recorded here as secondary phase, but in a very low amount comparing with BiFeO_3 phase, in contrast with the sample BFO4 where BiFeO_3 appears to be as secondary phase. In addition, by comparing BFO4 and BFO5, samples with the same Bi/Fe nominal ratio but differences in synthesis precursors, one can observe that stoichiometric BiFeO_3 phase (PDF #71-2494) is dominant in BFO5 sample. It is also evident that the three main diffraction peaks (*hkl* 012, 104, and 110) of the stoichiometric BiFeO_3 phase (PDF #71-2494) are now clearly visible in the sample's BFO5 diffraction pattern. Correspondingly, the respective intensities of BFO5 sample's diffraction pattern peaks agree with the reference peak intensities of the stoichiometric BiFeO_3 phase, as shown by olive-color vertical lines in Figure 1b.

Figure 2a shows the X-ray diffractograms of the annealed BFO sample (BFO5) in nominal Bi/Fe molar ratio (1/1) together with reference as prepared sample (BFO6). Regarding the reference sample BFO6, the presence of bismuth oxide phases (Bi_2O_3 ; PDF #45-1344 and #51-1161, blue and green colors, respectively) is unavoidable as clearly shown with blue and green vertical lines, under spectra (Figure 2a), respectively. On the contrary, the desirable target phase of bismuth iron oxide (BiFeO_3) is dominant (PDF #71-2494, olive-colored lines) without any presence of bismuth oxides after 2 h annealing under Ar atmosphere at calcination temperature of 700 °C. It has been previously confirmed by several works^[1,27,43] that the pure BFO phase without any impurities and secondary phases could be obtained only when the calcination temperature is close to 700 °C.

Microstructural characterization of the multiferroic samples, performed by a droplet of 1 mg mL⁻¹ solution upon a silicon substrate, is shown in Figure 2b,c, SEM images of the prepared BFO samples before (BFO6—Figure 2b, left brown-color box) and after (BFO5—Figure 2c, right pink-color box) annealing. Interestingly, large (>1 μm in diameter) multifaceted particles were observed before annealing (BFO6 samples), whereas smaller (<1 μm in diameter) cubic-like particles with smoother faces and clearer edges are formed after 2 h annealing at 700 °C at Ar atmosphere (BFO5 sample). Similar effects of annealing on morphology have been reported previously by Park et al.^[26] for 600 °C annealing temperature. This difference in morphology between before and after annealed samples (BFO6 and BFO5

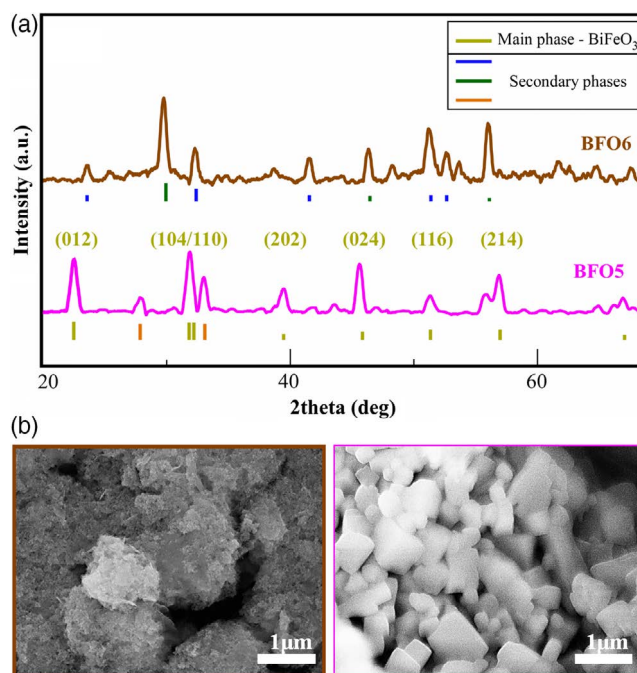


Figure 2. a) X-ray diffractograms of the annealed BFO sample (BFO5) in nominal Bi/Fe molar ratio (1/1) together with its reference sample (BFO6) before annealing. SEM images of the two samples c) BFO5 and b) BFO6 demonstrating the change in morphology after the 2 h calcination at 700 °C under Ar atmosphere.

samples, respectively) may be attributed to the diminishing of the secondary impurity Bi oxide phases (Bi_2O_3) hindering the high content of single-phase NPs. Typically, BiFeO_3 is accompanied by secondary phases such as $\text{Bi}_2\text{Fe}_4\text{O}_9$ and $\text{Bi}_{25}\text{FeO}_{29}$.^[44,45] Probably, the impurity phases in the XRD patterns correspond to the volatilization of Bi^{3+} ions which result due to excess addition of Bi.

By measuring the full width at half maximum of the four strongest diffraction peaks and using elemental analysis with EDX detection, the Bi/Fe atomic ratio is estimated for each sample as shown in Table 1 in comparison with the respective initial Bi/Fe molar ratio used in the synthesis. As it is expected, BFO1 sample with initial Bi/Fe molar ratio at 1/3 has the highest Fe content with 0.61 Bi/Fe atomic ratio. On the contrary, initial Bi/Fe molar ratio of 3/1 and 1/1, used in samples BFO2 and BFO3, BFO4, BFO5, BFO6, respectively, resulted in a Bi content excess as shown in third column of Table 1. Interestingly, bismuth atomic content in BFO2 sample is more than 5 times greater than iron atomic content (Bi/Fe atomic ratio is 5.4 as shown in Table 1), explaining the strong existence of the bismuth enhanced impurity phase of $\text{Bi}_{46}\text{Fe}_2\text{O}_{72}$ (PDF #20-0170). It should be noted that this deviation from 1/1 Bi/Fe atomic ratio in BFO3, BFO4, BFO5, and BFO6 samples can explain the several secondary phases that XRD results revealed (Figure 1 and 2a) for these samples. In addition, BFO5 sample has the closer to 1/1 Bi/Fe atomic ratio (1.4) comparing with the other three nominal 1/1 Bi/Fe molar ratio samples (BFO3, BFO4, and BFO6 with 1.7, 1.8, and 1.6 Bi/Fe atomic ratio, respectively) and this

explains why, in XRD diffraction patterns, the stoichiometric phase of BiFeO₃ (PDF #71-2494, olive-colored lines in Figure 1 and 2a) appears as the dominant phase. It should be mentioned here that even though BFO3 and BFO4 samples have similar atomic Bi/Fe ratio (1.7 and 1.8, as shown in Table 1, respectively) their crystallite sizes are strongly different (BFO4 NPs have a twice larger crystallite size [42 nm] than BFO3 [19 nm]). This may be attributed to the difference in temperature reaction during synthesis (83 and 70 °C in case of BFO3 and BFO4 sample synthesis, respectively) as well as to the pH level reached in each case (12 and 10 for BFO3 and BFO4 samples, respectively). It has been shown^[28] that pH levels during the synthesis of BFO NPs has direct impact, yet there is a literature gap on this correlation. Meanwhile, most literature reports,^[23,26,28] focusing on the synthesis of BFO NPs, use pH synthesis values up to 11 which is less than pH value of 12 we used for the preparation of BFO3 sample and of the best, from structural point of view, BFO5 sample. Regarding this work's results and according to XRD patterns of Figure 1, we propose pH level of 12 as the optimum synthesis condition for the preparation of pure bismuth ferrite NPs. In addition, annealing temperature appears in several works as the most crucial synthesis factor strongly affecting the size of BFO NPs.^[26] Regarding Figure 1, one can also state that the presence of secondary Bi iron oxide phases is more evident in BFO4 than in BFO3, which is a result of the different synthesis parameters followed as discussed before and can also be a reason of the observed size difference. In contrast, pure BFO5 sample shows a mean crystallite size of 38 nm which has also been suggested previously^[26] as the optimum mean size of bismuth ferrite NPs to present unique multiferroic properties.

It is well known from the literature that the secondary phases in BFO NPs can also affect their magnetic properties^[5,46] and it has been extensively mentioned that it is impossible to avoid them at the final product.^[47] Moreover, the magnetic feature may arise due to the presence of oxygen defects.^[48–50] The presence of oxygen vacancies leads to the formation of Fe²⁺ to maintain charge balance in the material.^[46] In nanomaterial, the magnetic properties are associated to the structural strains that can lead to noncolinearity of spin and suppression of the spiral order. Theoretically, the effect of oxygen vacancies and strain on magnetic properties can be investigated using the principles density functional theory calculations.^[46] It is evident that the magnetic properties of BFO NPs are stronger at the small crystalline size. At lower crystalline size, the magnetic dipole moments interact strongly and show ferromagnetic behavior in ferrite. The magnetic properties are improved at lower crystalline size due to the suppression of cycloid structure, on the contrary, they are weakened at the higher size (for diameters larger than 65 nm).^[26,51] It is also worth to mention here that the magnetic properties of BFO are associated with Fe³⁺ spins occupying the B sites in the perovskite unit cell. More specifically, the ferromagnetic properties are associated to the partially filled d orbital of Fe³⁺ ion by Fe—O—Fe superexchange interactions.^[52,53] From the point of view of magnetic ordering, BFO is an antiferromagnet below the Néel temperature $T_N = 643$ K. By increasing the Fe³⁺ ion amount, the Fe—O—Fe superexchange effect becomes stronger, indicating that Fe³⁺

ions and low oxygen vacancies can play an active role in the BFO structure and can also affect the display of magnetic properties.^[52] In addition to that, it is known from the literature that leakage currents in BFO limit its applicability with the existence of secondary phases such as Bi₂Fe₄O₉, Bi₂₅FeO₄₀, Bi₂O₃, Fe₂O₃, valence fluctuations of Fe ions and oxygen vacancies, reported as the major reasons for the leaky behavior.^[54] Accordingly, in this work, the amount of the secondary phases in BiFeO₃ is limited by changing the Bi/Fe molar ratio with a direct impact on the magnetic properties.

To investigate the magnetic properties of the BFO particles, magnetic measurements were performed using VSM magnetometry. The magnetic response observed as a function of the applied magnetic field is correlated with the structural findings, whereas the magnetic features (saturation magnetization M_s and coercive field H_c) of each sample are collected in the last two columns of Table 1. **Figure 3** shows the magnetization as a function of the applied magnetic field (field range of ± 1 T) of the BFO powders at room temperature, also well known as magnetization hysteresis loop. As shown in Table 1 and Figure 3a,b, BFO samples with Bi excess (Bi/Fe atomic ratio >1 in samples BFO2, BFO3, BFO4, BFO5, and BFO6) present weaker saturation magnetization at 1 T (up to $0.4 \text{ A m}^2 \text{ kg}^{-1}$) with respect to sample BFO1 appearing as the magnetically strongest ($M_s = 5.3 \text{ A m}^2 \text{ kg}^{-1}$), in accordance with its Fe content excess (Bi/Fe atomic ratio = 0.6). Regarding the samples' coercivity, Figure 3b,d shows that BFO2 and BFO6 samples have the weakest coercive field among all samples, 0.5 and 0.2 mT, respectively. Meanwhile, the excess in Bi content (Bi/Fe atomic ratio equals to 5.4) in BFO2 sample favors a diamagnetic-like behavior, as the corresponding green curve in Figure 3a shows.

As expected, BFO NPs with small crystallite size (<20 nm), such as BFO3 sample, present improved magnetic properties (M_s for BFO3 sample NPs was recorded at $0.4 \text{ A m}^2 \text{ kg}^{-1}$) compared with larger (>30 nm) crystallite size samples (BFO4, BFO5, and BFO6 samples present M_s values lower than $0.2 \text{ A m}^2 \text{ kg}^{-1}$).

The presence of the non-magnetic Bi oxide phases (blue and green peak-corresponded lines in Figure 2a), appearing in the not annealed BFO6 sample (Bi/Fe atomic ratio = 1.59), can explain its weak M_s and H_c values (orange curves in Figure 3c,d). The improved phase of BFO5 sample (the undesirable bismuth oxide phases of BFO6 sample no longer exist in BFO5 with Bi/Fe atomic ratio = 1.40, as XRD results show in Figure 2a), revealed after the annealing process, has a direct positive impact on its magnetic features. The significance of this result is even more emphasized by the fact that, according to the literature reports,^[20,27,28] aqueous coprecipitation, used as a synthesis method for bismuth ferrite NPs, results in nonpure BiFeO₃ NPs, with a strong presence of Bi oxide phases in the final product. Interestingly, regarding the crystallite sizes of this work's samples and their connection with the respective magnetic properties, one can see from Table 1 that BFO5 sample presents a coercivity of 32 mT and an M_s of $0.2 \text{ A m}^2 \text{ kg}^{-1}$ for a crystallite size of 38 nm. Analogous magnetic behavior with the best, from structural point of view sample (as in the case of BFO5), has also been reported.^[26] More specifically, Park et al. showed in their

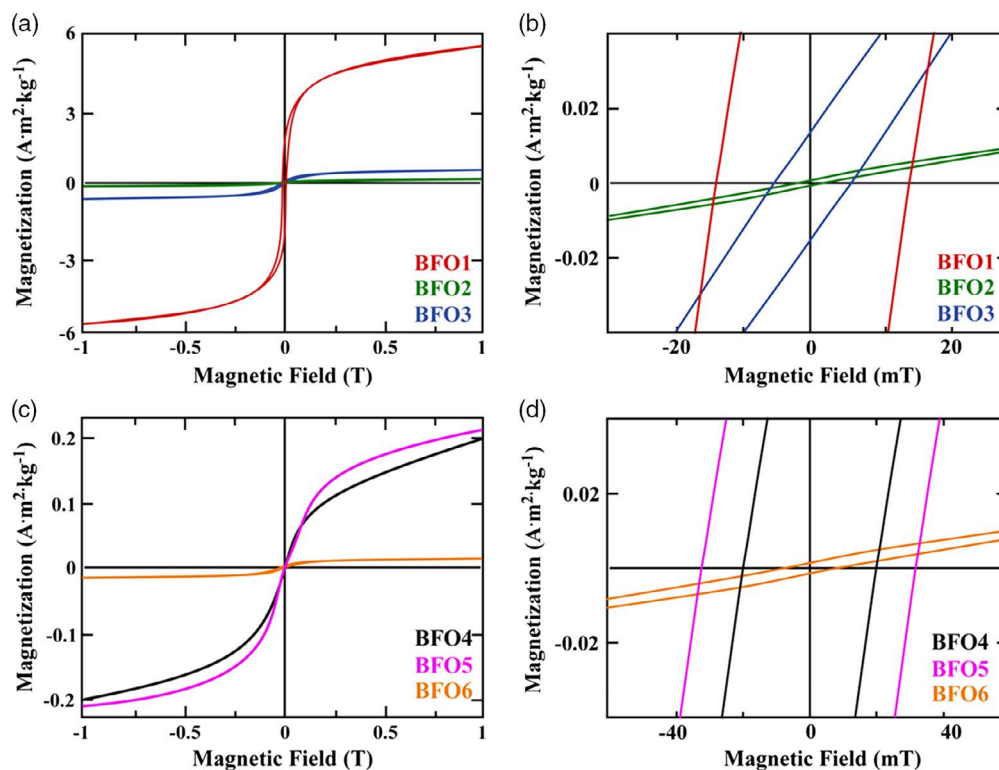


Figure 3. Hysteresis loops at 300 K for a) BFO samples synthesized using different nominal Bi/Fe molar ratio (BFO1 [1/3], BFO2 [3/1], and BFO3 [1/1]) and annealed at 700 °C for 2 h and c) BFO samples synthesized using different precursors, under the same nominal Bi/Fe molar ratio (1/1) with BFO4 and BFO5 annealed at 700 °C under Ar atmosphere for 2 h and with reference as-prepared BFO6 sample; b,d) with rescaled axis depicting the respective coercivity for all samples.

work that BiFeO₃ MNPs of 41 nm (comparable with BFO5 sample with size of 38 nm) possessed a coercive field value of 30.5 mT, which is very similar to BFO5 sample's coercivity. In addition, similar saturation magnetization to BFO5 sample has been reported in the work of Carranza-Celis et al.^[19] More specifically, sol-gel synthesis method was proposed to form BFO NPs at 600 °C. Room temperature hysteresis loop exhibited superparamagnetic-like behavior with a very weak ferromagnetic component, with a 2.2 mT coercive field and similar to BFO5 M_s at 0.17 A m² kg⁻¹. It should be noted here that different synthesis procedure may impact the final structural and magnetic properties of the products. More specifically, Carranza-Celis et al. suggested in their work^[19] that annealing temperature may have a crucial impact not only to the structure of the BFO NPs but to their magnetic properties as well. Interestingly, after applying linear extrapolation on their experimental magnetization data, Park et al.^[26] suggested that the highest magnetization achievable for substrate-free BiFeO₃ NPs, ranging in size diameter from 14 to 75 nm, can attain values of up to about 1.82 A m² kg⁻¹. To put this value into context, magnetization values of 1.00–1.66 A m² kg⁻¹ for epitaxially grown BiFeO₃ thin films have been previously reported.^[55,56]

Despite the weak M_s value of BFO5 NPs sample, which can be attributed to secondary phase BFO contents and the Bi excess, its structural and magnetic properties are apparently improved compared with the rest of the samples, indicating that the exploration

and evaluation of each synthesis parameter may lead to the BFO sample with tunable structural and magnetic properties.

4. Conclusions

BiFeO₃ NPs were formed using aqueous coprecipitation method followed by 2 h annealed at Ar atmosphere at 700 °C. The investigation of three different Bi/Fe molar ratios (1/3, 3/1, and 1/1) and their impact to the final BFO product highlight the 1/1 as the optimum, both from structural and magnetic point of view, Bi/Fe ratio. Furthermore, the occurrence of impurity phases in the final BFO product can be controlled by simple synthetic steps. At the same time, structural and magnetic properties of not-annealed and postannealed BFO samples reveal the significance of annealing procedure on forming BiFeO₃ with attenuating secondary BFO content which is crucial to bring out the unique magnetoelectric properties.

Acknowledgements

This research was funded in the context of the project “Exploitation of field effects on appropriate nanoparticulate carriers for modern biomedical applications” (MIS 5005039) under the call for proposals “Supporting researchers with emphasis on new researchers” (EDULLL 34). The project was cofinanced by Greece (Greek national funds) and the European Union

(European Social Fund [ESF]) by the Operational Programme “Human Resources Development, Education and Lifelong Learning” (2014–2020).

Conflict of Interest

The authors declare no conflict of interest.

Keywords

BiFeO₃, bismuth ferrite, coprecipitation, magnetoelectric, multiferroic

Received: January 2, 2020

Revised: March 3, 2020

Published online: March 20, 2020

- [1] L. W. Martin, S. P. Crane, Y. H. Chu, M. B. Holcomb, M. Gajek, M. Huijben, C. H. Yang, N. Balke, R. Ramesh, *J. Phys.: Condens. Matter* **2008**, *20*, 434220.
- [2] M. Fiebig, T. Lottermoser, D. Meier, M. Trassin, *Nat. Rev. Mater.* **2016**, *1*, 16046.
- [3] G. Catalan, J. F. Scott, *Adv. Mater.* **2009**, *21*, 2463.
- [4] T. Rojac, A. Bencan, B. Malic, G. Tutuncu, J. L. Jones, J. E. Daniels, D. Damjanovic, *J. Am. Ceram. Soc.* **2014**, *97*, 1993.
- [5] J. B. N. J. Wang, J. B. Neaton, H. Zheng, V. Nagarajan, S. B. Ogale, B. Liu, D. Viehland, V. Vaithyanathan, D. G. Schlom, U. V. Waghmare, N. A. Spaldin, *Science* **2003**, *299*, 1719.
- [6] J. R. Teague, R. Gerson, W. J. James, *Solid State Commun.* **1970**, *8*, 1073.
- [7] J. Wu, Z. Fan, D. Xiao, J. Zhu, J. Wang, *Prog. Mater. Sci.* **2016**, *84*, 335.
- [8] J. Wu, *Advances in Lead-Free Piezoelectric Materials*, Springer, New York, NY **2018**.
- [9] T. Zheng, C. Zhao, J. Wu, K. Wang, J. F. Li, *Scr. Mater.* **2018**, *155*, 11.
- [10] Y. P. Wang, G. L. Yuan, X. Y. Chen, J. M. Liu, Z. G. Liu, *J. Phys. D: Appl. Phys.* **2006**, *39*, 2019.
- [11] T. Choi, S. Lee, Y. J. Choi, V. Kiryukhin, S. W. Cheong, *Science* **2009**, *324*, 63.
- [12] A. P. Pyatakov, A. K. Zvezdin, *Phys. Usp.* **2012**, *55*, 557.
- [13] S. Li, R. Nechache, C. Harnagea, L. Nikolova, F. Rosei, *Appl. Phys. Lett.* **2012**, *101*, 192903.
- [14] A. Rajae, X. Wensheng, L. Zhao, S. Wang, Y. Liu, Z. Wu, J. Wang, F. Si-Shen, *J. Biomed. Nanotechnol.* **2018**, *14*, 1159.
- [15] A. Maitre, M. Francois, J. C. Gachon, *J. Phase Equilib. Diffus.* **2004**, *25*, 59.
- [16] R. Haumont, R. Saint-Martin, C. Byl, *Phase Transit.* **2008**, *81*, 881.
- [17] J. Silva, A. Reyes, H. Esparza, H. Camacho, L. Fuentes, *Integr. Ferroelectr.* **2011**, *126*, 47.
- [18] J. Lu, L. J. Qiao, P. Z. Fu, Y. C. Wu, *J. Cryst. Growth* **2011**, *318*, 936.
- [19] D. Carranza-Celis, A. Cardona-Rodríguez, J. Narváez, O. Moscoso-Londono, D. Muraca, M. Knobel, N. Ornelas-Soto, A. Reiber, J. G. Ramírez, *Sci. Rep.* **2019**, *9*, 3182.
- [20] M. I. Morozov, N. A. Lomanova, V. V. Gusarov, *Russ. J. General Chem.* **2003**, *73*, 1676.
- [21] S. M. Selbach, M. A. Einarsrud, T. Grande, *Chem. Mater.* **2008**, *21*, 169.
- [22] S. Phapale, R. Mishra, D. Das, *J. Nucl. Mater.* **2008**, *373*, 137.
- [23] F. Huang, Z. Wang, X. Lu, J. Zhang, K. Min, W. Lin, R. Ti, T. Xu, J. He, C. Yue, J. Zhu, *Sci. Rep.* **2013**, *3*, 2907.
- [24] M. Valant, A. K. Axelsson, N. Alford, *Chem. Mater.* **2007**, *19*, 5431.
- [25] I. O. T. I. Sosnowska, W. Schäfer, W. Kockelmann, K. H. Andersen, I. O. Troyanchuk, *Appl. Phys. A* **2002**, *74*, 1042.
- [26] T. J. Park, G. C. Papaefthymiou, A. J. Viescas, A. R. Moodenbaugh, S. S. Wong, *Nano Lett.* **2007**, *7*, 766.
- [27] N. A. Lomanova, V. V. Gusarov, *Nanosyst.: Phys. Chem. Math.* **2012**, *3*, 112.
- [28] M. Muneeswaran, P. Jegatheesan, N. V. Giridharan, *J. Exp. Nanosci.* **2013**, *8*, 341.
- [29] E. A. V. Ferri, I. A. Santos, E. Radovanovic, R. Bonzanini, E. M. Giroto, *J. Braz. Chem. Soc.* **2008**, *19*, 1153.
- [30] K. Chybczynska, M. Blaszyk, B. Hilczer, T. Lucinski, M. Matczak, B. Andrzejewski, *Mater. Res. Bull.* **2017**, *86*, 178.
- [31] S. Riaz, S. M. H. Shah, A. Akbar, Z. N. Kayani, S. Naseem, *IEEE Trans. Magn.* **2014**, *50*, 1.
- [32] J. H. Xu, H. Ke, D. C. Jia, W. Wang, Y. Zhou, *J. Alloys Compd.* **2009**, *472*, 473.
- [33] B. Liu, B. Hu, Z. Du, *Chem. Commun.* **2011**, *47*, 8166.
- [34] A. Gajović, S. Šturm, B. Jančar, A. Šantić, K. Žagar, M. Čeh, *J. Am. Ceram. Soc.* **2010**, *93*, 3173.
- [35] M. Popa, D. Crespo, J. M. Calderon-Moreno, S. Preda, V. Fruth, *J. Am. Ceram. Soc.* **2007**, *90*, 2723.
- [36] A. Hardy, S. Gielis, H. Van den Rul, J. D’Haen, M. K. Van Bael, J. Mullens, *J. Eur. Ceram. Soc.* **2009**, *29*, 3007.
- [37] A. V. Mikhailov, N. A. Gribchenkova, E. N. Kolosov, A. S. Alikhanyan, *Russ. J. Phys. Chem. A* **2011**, *85*, 26.
- [38] S. Shetty, V. R. Palkar, R. Pinto, *Pramana* **2002**, *58*, 1027.
- [39] J. Yang, X. Li, J. Zhou, Y. Tang, Y. Zhang, Y. Li, *J. Alloys Compd.* **2011**, *509*, 9271.
- [40] J. Prado-Gonjal, M. E. Villafuerte-Castrejón, L. Fuentes, E. Moran, *Mater. Res. Bull.* **2009**, *44*, 1734.
- [41] V. Kothai, R. Ranjan, *Bull. Mater. Sci.* **2012**, *35*, 157.
- [42] B. Jurca, C. Paraschiv, A. Ianculescu, O. Carp, *J. Therm. Anal. Calorim.* **2009**, *97*, 91.
- [43] H. Maleki, M. Haselpour, R. Fathi, *J. Mater. Sci. Mater. Electron.* **2018**, *29*, 4320.
- [44] I. Sosnowska, T. P. Neumaier, E. Steichele, *J. Phys. C: Solid State Phys.* **1982**, *15*, 4835.
- [45] V. Srinivas, A. T. Raghavender, K. V. Kumar, *Phys. Res. Int.* **2016**, *2016*, 1.
- [46] C. Ederer, N. A. Spaldin, *Phys. Rev. B* **2005**, *71*, 224103.
- [47] V. Berbenni, C. Milanese, G. Bruni, A. Girella, A. Marini, *Ceram. Int.* **2015**, *41*, 7216.
- [48] A. Tamilselvan, S. Balakumar, M. Sakar, C. Nayek, P. Murugavel, K. S. Kumar, *Dalton Trans.* **2014**, *43*, 5731.
- [49] Q. Zhang, D. Sando, V. Nagarajan, *J. Mater. Chem. C* **2016**, *4*, 4092.
- [50] A. M. Afzal, M. Umair, G. Dastgeer, M. Rizwan, M. Z. Yaqoob, R. Rashid, H. S. Munir, *J. Magn. Magn. Mater.* **2016**, *399*, 77.
- [51] J. M. Moreau, C. Michel, R. Gerson, W. J. James, *J. Phys. Chem. Solids* **1971**, *32*, 1315.
- [52] J. Qi, Y. Zhang, Y. Wang, Y. Liu, M. Wei, J. Zhang, M. Feng, J. Yang, *J. Mater. Sci. Mater. Electron.* **2017**, *28*, 17490.
- [53] V. R. Palkar, J. John, R. Pinto, *Appl. Phys. Lett.* **2002**, *80*, 1628.
- [54] G. Rojas-George, A. Concha-Balderrama, J. Silva, L. Fuentes, A. Reyes-Rojas, *Ceram. Int.* **2015**, *41*, 9140.
- [55] W. Eerenstein, F. D. Morrison, J. Dho, M. G. Blamire, J. F. Scott, N. D. Mathur, *Science* **2005**, *307*, 1203.
- [56] H. Béa, M. Bibes, A. Barthélémy, K. Bouzehouane, E. Jacquet, A. Khodan, J. P. Contour, S. Fusil, F. Wyczisk, A. Forget, D. Lebeugle, *Appl. Phys. Lett.* **2005**, *87*, 072508.